A new composite scheme for two-layer shallow water flows with shocks

Nouh Izem[1,†]   Fayssal Benkhaldoun[‡]   Slah Sahmim[§]
Mohammed Seaid[¶]   Mohamed Wakrim[‖]

Abstract

This paper is devoted to solve the system of partial differential equations governing the flow of two superposed immiscible layers of shallow water flows. The system contains source terms due to bottom topography, wind stresses, and nonconservative products describing momentum exchange between the layers. The presence of these terms in the flow model forms a nonconservative system which is only conditionally hyperbolic. In addition, two-layer shallow water flows are often accompanied with moving discontinuities and shocks. Developing stable numerical methods for this class of problems presents a challenge in the field of computational hydraulics. To overcome these difficulties, a new composite scheme is proposed. The scheme consists of a time-splitting operator where in the first step the homogeneous system of the governing equations is solved using an approximate Riemann solver. In the second step a finite volume method is used to update the solution. To remove the non-physical oscillations in the vicinity of shocks a nonlinear filter is applied. The method is well-balanced, non-oscillatory and it is suitable for both low and high values of the density ratio between the two layers. Several standard test examples for two-layer shallow water flows are used to verify high accuracy and good resolution properties for smooth and discontinuous solutions.

Keywords. Two-layer shallow water equations, Nonconservative systems, Finite volume method, Riemann solver, Nonlinear filter.

1   Introduction

In the present study we consider the two-layer shallow water system of partial differential equations governing the one-dimensional flow of two superposed shallow layers of immiscible fluids with different constant densities, ρ_1 and ρ_2 ($\rho_1 < \rho_2$), due to, for example, different water temperature or salinity. The mathematical equations are derived from the compressible isentropic Euler equations by vertical averaging across each layer depth, see [3, 4] among others.

[1]Correspondence to: izemnouh@gmail.com
[†]EMMS Faculty of science, Ibn Zohr University Agadir, Morocco
[‡]LAGA, Université Paris 13, 99 Av J.B. Clement, 93430 Villetaneuse, France
[§]Laboratoire D'ingénierie Mathématique, Ecole Polytechnique de Tunisie, Tunisia
[¶]School of Engineering and Computing Sciences, University of Durham, South Road, Durham DH1 3LE, UK
[‖]EMMS Faculty of science, Ibn Zohr University Agadir, Morocco
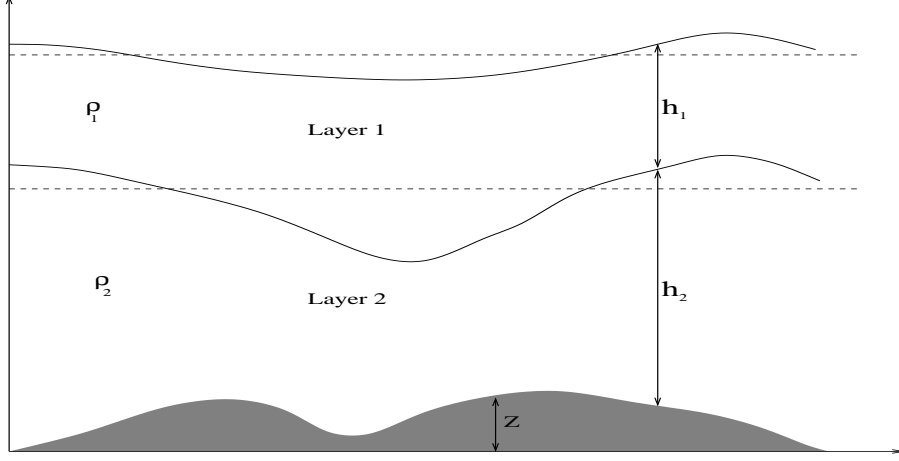
Figure 1: Schematic of a two-layer shallow model with topography.

The model reads

$$\frac{\partial h_1}{\partial t} + \frac{\partial (h_1 u_1)}{\partial x} = 0,$$

$$\frac{\partial (h_1 u_1)}{\partial t} + \frac{\partial}{\partial x}\left(h_1 u_1^2 + \frac{1}{2}gh_1^2\right) = -gh_1\frac{\partial}{\partial x}(Z + h_2) + \mathcal{F}_w,$$

$$\frac{\partial h_2}{\partial t} + \frac{\partial (h_2 u_2)}{\partial x} = 0,$$

$$\frac{\partial (h_2 u_2)}{\partial t} + \frac{\partial}{\partial x}\left(h_2 u_2^2 + \frac{1}{2}gh_2^2\right) = -gh_2\frac{\partial}{\partial x}\left(Z + \frac{\rho_1}{\rho_2}h_1\right) + \mathcal{F}_b,$$

(1)

where ρ_j is the water density of the jth layer, $h_j(t, x)$ is the water height of the jth layer, $u_j(t, x)$ is the local water velocity for the jth layer, $j = 1, 2$, $Z(x)$ is the bottom topography and g the gravitational acceleration. Here, the subscripts 1 and 2 represent respectively, the upper and lower layer in the hydraulic system, see Figure 1 for an illustration. In (1), the bed friction forcing term $\mathcal{F}_b$ is acting only on the lower layer and the wind-driven forcing term $\mathcal{F}_w$ is acting only on the upper layer as

$$\mathcal{F}_b = -\frac{\tau_b}{\rho_2}, \qquad \mathcal{F}_w = \frac{\tau_\omega}{\rho_1}, \qquad (2)$$

with τ_b and τ_ω are respectively, the bed shear stress and the shear of the blowing wind defined by the water and wind velocities as

$$\tau_b = \rho_2 C_b u_2 |u_2|, \qquad \tau_\omega = \rho_1 C_\omega \omega |\omega|, \qquad (3)$$

where C_b is the bed friction coefficient, which may be either constant or estimated as $C_b = g/C_z^2$, where $C_z = h_2^{1/6}/nb$ is the Chezy constant, with nb being the Manning roughness coefficient at the bed. In (3) ω is the velocity of wind at 10 m above water surface and C_w is the coefficient of wind friction defined as [1]

$$C_w = \rho_a(0.75 + 0.067|\omega|) \times 10^{-3},$$

where ρ_a is the air density. It is well known that the calculation of the eigenvalues associated with the two-layer system (1) is not trivial. Indeed, the four eigenvalues λ_j $(j = 1, \ldots, 4)$ are the zeros of the characteristic polynomial [4]

$$P(\lambda) = \left(\lambda^2 - 2u_1\lambda + u_1^2 - gh_1\right)\left(\lambda^2 - 2u_2\lambda + u_2^2 - gh_2\right) - g^2 rh_1 h_2, \qquad (4)$$

2

where the ratio $r = \frac{\rho_1}{\rho_2}$. Notice that for hydraulic applications with $r \approx 1$ and $u_1 \approx u_2$, a first-order approximation of the eigenvalues can be obtained by expanding (4) in terms of $1 - r$ and $u_2 - u_1$ as

$$
\begin{aligned}
\lambda_1 &\approx U_m - \sqrt{g\left(h_1 + h_2\right)}, \\
\lambda_2 &\approx U_m + \sqrt{g\left(h_1 + h_2\right)}, \\
\lambda_3 &\approx U_c - \sqrt{(1-r)g\frac{h_1 h_2}{h_1 + h_2}\left(1 - \frac{(u_2 - u_1)^2}{(1-r)g\left(h_1 + h_2\right)}\right)}, \\
\lambda_4 &\approx U_c + \sqrt{(1-r)g\frac{h_1 h_2}{h_1 + h_2}\left(1 - \frac{(u_2 - u_1)^2}{(1-r)g\left(h_1 + h_2\right)}\right)},
\end{aligned}
\tag{5}
$$

where

$$
U_m = \frac{h_1 u_1 + h_2 u_2}{h_1 + h_2}, \qquad U_c = \frac{h_1 u_2 + h_2 u_1}{h_1 + h_2}.
$$

It is evident that, depending on the values of the ratio r, the eigenvalues (5) may become complex, see for instance [10]. In this case, the system is not hyperbolic and yields to the so-called Kelvin-Helmholtz instability at the interface separating the two layers. A necessary condition for the system (1) to be hyperbolic is

$$
\frac{(u_1 - u_2)^2}{(1-r)g\left(h_1 + h_2\right)} < 1.
\tag{6}
$$

It should also be stressed that if $\rho_1 = \rho_2$, $u_1 = u_2 = u$ and $h_1 + h_2 = H$ the system (1) reduces to the canonical single-layer shallow water equations

$$
\begin{aligned}
\frac{\partial H}{\partial t} + \frac{\partial\left(Hu\right)}{\partial x} &= 0, \\
\frac{\partial\left(Hu\right)}{\partial t} + \frac{\partial}{\partial x}\left(Hu^2 + \frac{1}{2}gH^2\right) &= -gH\frac{\partial Z}{\partial x} + \mathcal{F}_b + \mathcal{F}_w,
\end{aligned}
\tag{7}
$$

Note that the system (7) forms a conservative hyperbolic with two real eigenvalues given by $\lambda_1 = u - \sqrt{gh}$ and $\lambda_2 = u + \sqrt{gh}$.

The two-layer shallow water equations (1) have been widely used in the literature as a prototype of nonconservative hyperbolic systems, see for example [4, 12]. These equations have also been presented as a model of conservation laws with a severe restriction on the hyperbolicity in [2, 13] among others. Recent trends in modeling multi-layer shallow water flows consist in the inclusion of other physical mechanisms such as sediment transport, compare [14]. The numerical solution of two-layer shallow water equations has also been object of an intense research during the last years, see for instance [11, 6]. This interest is due, on the one hand, to the applicability of these models to the simulation of stratified geophysical flows. On the other hand, they can be considered as a prototype of partial differential equations involving similar difficulties, as it is the case for a number of two-phase flow models. One of the main difficulties of system (1) both from the theoretical and the numerical point of views comes from the presence of nonconservative products. Thus, solutions of (1) may develop discontinuities and, due to the non-divergence form of the equations, the notion of weak solution in the sense of distributions cannot be used. A second important difficulty of system (1) is related to the loss of hyperbolicity when the density ratio r approaches unity. Indeed, when $r \cong 1$ the condition (6) may be violated and the system (1) is only conditionally hyperbolic. In this situation, its

eigenstructure cannot be obtained in an explicit form. This loss of hyperbolicity is related to the appearance of shear instabilities that may lead, in real flows, to intense mixing of the two layers. While, in practice, this mixture partially dissipates the energy, in numerical experiments these interface disturbances may grow and overwhelm the solution. Even though these factors make it quite difficult to design upwind methods for the two-layer shallow water equations. For instance, several upwind-based schemes, including the finite-volume [4, 12] and finite-element [11] ones, were developed during the past decade. An interesting approach to overcome the above difficulties has been recently proposed in [6], where two artificial equations have been added to the system (1), so that the extended system becomes hyperbolic and thus could be solved by a second-order Roe-type scheme in a rather straightforward manner. Time splitting approaches, proposed for example in [2], are another way to implement upwinding without having the full eigenstructure of the system readily available. The main objective of this work is to reconstruct a non-oscillatory method to accurately approximate numerical solutions of the two-layer shallow water flows over non-flat beds. In the current study we propose a new composite finite volume method for solving the two-layer shallow water equations (1). The key idea in this approach is to apply a time-splitting operator to the governing equations where the homogeneous system is solved using an approximate Riemann solver developed in [16] and the source terms are dealt with in the second stage of the time-splitting procedure. In order to increase the resolution of the scheme and remove undesirable oscillations near the shocks a nonlinear filter is applied. The proposed method is non-oscillatory and suitable for two-layer shallow water equations for which Riemann problems are difficult to solve. Numerical examples are presented to verify the considered composite method. We demonstrate the method capability of capturing the shocks and calculating lateral and vertical distributions of velocities for wind-driven circulation over complex bathymetry.

The remainder of this paper is organized as follows. In section 2 we present the composite scheme for the two-layer shallow water equations. This section includes both the discretization of gradient fluxes and formulation of the nonlinear filter. Section 3 contains numerical results and examples. Concluding remarks are summarized in section 4.

2 A new composite scheme

For simplicity in presentation we rewrite the two-layer equations (1) in a compact form as

$$\frac{\partial \mathbf{W}}{\partial t} + \frac{\partial \mathbf{F}(\mathbf{W})}{\partial x} = \mathbf{Q}(\mathbf{W}) + \mathbf{R}(\mathbf{W}), \tag{8}$$

where $\mathbf{W}$ is the vector of conserved variables, $\mathbf{F}$ the vector of flux functions, $\mathbf{Q}$ and $\mathbf{R}$ are the vectors of source terms defined by

$$\mathbf{W} = \begin{pmatrix} h_1 \\ h_1 u_1 \\ h_2 \\ h_1 u_2 \end{pmatrix}, \qquad \mathbf{F}(\mathbf{W}) = \begin{pmatrix} h_1 u_1 \\ h_1 u_1^2 + \dfrac{1}{2} g h_1^2 \\ h_2 u_2 \\ h_2 u_2^2 + \dfrac{1}{2} g h_2^2 \end{pmatrix},$$

$$\mathbf{Q}(\mathbf{W}) = \begin{pmatrix} 0 \\ -g h_1 \dfrac{\partial}{\partial x} (Z + h_2) \\ 0 \\ -g h_2 \dfrac{\partial}{\partial x} (Z + r h_1) \end{pmatrix}, \qquad \mathbf{R}(\mathbf{W}) = \begin{pmatrix} 0 \\ \dfrac{\tau_\omega}{\rho_1} \\ 0 \\ -\dfrac{\tau_b}{\rho_2} \end{pmatrix}.$$

4

It is well-established that the source terms in (8) are stiff such that implementing them directly causes an instability as it was shown [15] for a simple explicit discretization of source term integrated in the finite volume scheme for single-layer shallow water model. To overcome this drawback, a numerical time-splitting method obtained by performing an arbitrary scheme, in this case a nonhomogeneous Riemann solver, is used.

Let the temporal domain be divided into subintervals $[t_n, t_{n+1}]$ with stepsize Δt. We used the notation $\mathbf{W}^n$ to denote the solution $\mathbf{W}$ at time $t = t_n$. In the simplest case, this splitting takes the following form

$$\mathbf{W}^{n+1} = \mathcal{L}_{\mathbf{Q}}^{\Delta t} \mathcal{L}_{\mathbf{F}}^{\Delta t} \mathcal{L}_{\mathbf{R}}^{\Delta t} \mathbf{W}^n, \tag{9}$$

where $\mathcal{L}_{\mathbf{F}}^{\Delta t}$ represents the numerical solution operator for the conservation law

$$\frac{\partial \mathbf{W}}{\partial t} + \frac{\partial \mathbf{F}(\mathbf{W})}{\partial x} = \mathbf{0}, \tag{10}$$

over the time Δt, $\mathcal{L}_{\mathbf{R}}^{\Delta t}$ and $\mathcal{L}_{\mathbf{Q}}^{\Delta t}$ are the numerical solution operators for the equations of source terms

$$\frac{\partial \mathbf{W}}{\partial t} = \mathbf{R} \qquad \text{and} \qquad \frac{\partial \mathbf{W}}{\partial t} = \mathbf{Q},$$

respectively. It should be stressed that, although this fractional scheme (known as strong splitting) performs well for the two-layer shallow water equations over flat bottom, highly oscillations can be detected close to the shock areas when it is applied to two superposed immiscible layers of shallow water over non-flat bottom.

It is worth emphasizing that, using the two-layer equations to model shallow water flows, the nonhomogenuous terms in the right-hand side in (1) are not standard source terms but nonconservative products, since they include derivatives of two of the variables. The presence of these source terms in the two-layer shallow water systems can cause severe difficulties in their numerical approximations, see for instance [8]. In principle, the nonhomegenuous term in these equations can be viewed as a source term and/or a nonconservative term. In the approach presented in this study these terms are considered and discretized as source terms.

2.1 A well-balanced finite volume method

The homogeneous system (10) can be numerically solved using any finite volume method designed for hyperbolic systems of conservation laws. In the current work we employ an approximate Riemann solver developed in [16] among others. The method consists of a predictor stage for the discretization of gradient terms and a corrector stage for the finite volume solution recovery. The numerical fluxes are reconstructed using a modified Roe's scheme that incorporates, in its reconstruction, the sign of the Jacobian matrix in the two-layer shallow water system. Herein, this method is referred to by SRNHS scheme, see for example [16]. In this section we briefly describe the method and details can be found in [16].

It is easy to verify that the eigenvalues λ_k $(k = 1, \ldots, 4)$ associated with the Jacobian matrix in (10) are given by

$$\begin{aligned} \lambda_1 &= u_1 + \sqrt{gh_1}, & \lambda_2 &= u_1 - \sqrt{gh_1}, \\ \lambda_3 &= u_2 + \sqrt{gh_2}, & \lambda_4 &= u_2 - \sqrt{gh_2}. \end{aligned} \tag{11}$$

Let us discretize the spatial domain into control volumes $[x_{i-1/2}, x_{i+1/2}]$ with uniform size $\Delta x = x_{i+1/2} - x_{i-1/2}$. Applied to the system (10) the finite volume SRNHS method is

$$\begin{aligned} \mathbf{W}_{i+1/2}^n &= \frac{1}{2}\left(\mathbf{W}_{i+1}^n + \mathbf{W}_i^n\right) - \frac{1}{2}\mathrm{sgn}\left[\mathbf{A}\left(\overline{\mathbf{W}}\right)\right]\left(\mathbf{W}_{i+1}^n - \mathbf{W}_i^n\right), \\ \mathbf{W}_i^{n+1} &= \mathbf{W}_i^n - \frac{\Delta t}{\Delta x}\left(\mathbf{F}\left(\mathbf{W}_{i+1/2}^n\right) - \mathbf{F}\left(\mathbf{W}_{i-1/2}^n\right)\right), \end{aligned} \tag{12}$$

where $\mathbf{W}_i^n$ is the space average of the solution $\mathbf{W}$ in the control volume $[x_{i-1/2}, x_{i+1/2}]$ at time t_n *i.e.*,

$$\mathbf{W}_i^n = \frac{1}{\Delta t \Delta x} \int_{t_n}^{t_{n+1}} \int_{x_{i-1/2}}^{x_{i+1/2}} \mathbf{W}(t,x) \, dt \, dx,$$

and $\mathbf{F}(\mathbf{W}_{i\pm1/2}^n)$ are the numerical fluxes at $x = x_{i\pm1/2}$ and time t_n. In (12), the averaged state is calculated as

$$\overline{\mathbf{W}} = \begin{pmatrix} \dfrac{h_{1,i} + h_{1,i+1}}{2} \\ \dfrac{h_{1,i} + h_{1,i+1}}{2} \dfrac{u_{1,i}\sqrt{h_{1,i}} + u_{1,i+1}\sqrt{h_{1,i+1}}}{\sqrt{h_{1,i}} + \sqrt{h_{1,i+1}}} \\ \dfrac{h_{2,i} + h_{2,i+1}}{2} \\ \dfrac{h_{2,i} + h_{2,i+1}}{2} \dfrac{u_{2,i}\sqrt{h_{2,i}} + u_{2,i+1}\sqrt{h_{2,i+1}}}{\sqrt{h_{2,i}} + \sqrt{h_{2,i+1}}} \end{pmatrix}, \tag{13}$$

and the sign matrix is given by

$$\mathrm{sgn}\Big[\mathbf{A}\left(\overline{\mathbf{W}}\right)\Big] = \mathcal{R}\left(\overline{\mathbf{W}}\right)\mathrm{sgn}\Big[\Lambda\left(\overline{\mathbf{W}}\right)\Big]\mathcal{R}^{-1}\left(\overline{\mathbf{W}}\right),$$

with

$$\mathrm{sgn}\Big[\Lambda\left(\overline{\mathbf{W}}\right)\Big] = \begin{pmatrix} \mathrm{sgn}\left(\overline{\lambda}_1\right) & 0 & 0 & 0 \\ 0 & \mathrm{sgn}\left(\overline{\lambda}_2\right) & 0 & 0 \\ 0 & 0 & \mathrm{sgn}\left(\overline{\lambda}_3\right) & 0 \\ 0 & 0 & 0 & \mathrm{sgn}\left(\overline{\lambda}_4\right) \end{pmatrix},$$

where $\overline{\lambda}_k$ are the eigenvalues in (11) calculated at the averaged states. The right and left eigenvector matrices are given by

$$\mathcal{R}\left(\overline{\mathbf{W}}\right) = \begin{pmatrix} 1 & 0 & 0 & 0 \\ \overline{\lambda}_1 & \overline{\lambda}_2 & 0 & 0 \\ 0 & 0 & 1 & 1 \\ 0 & 0 & \overline{\lambda}_3 & \overline{\lambda}_4 \end{pmatrix}, \qquad \mathcal{R}^{-1}\left(\overline{\mathbf{W}}\right) = \begin{pmatrix} -\dfrac{\overline{\lambda}_2}{2c_1} & \dfrac{1}{2c_1} & 0 & 0 \\ \dfrac{\overline{\lambda}_1}{2c_1} & -\dfrac{1}{2c_1} & 0 & 0 \\ 0 & 0 & -\dfrac{\overline{\lambda}_4}{2c_2} & \dfrac{1}{2c_2} \\ 0 & 0 & \dfrac{\overline{\lambda}_3}{2c_2} & -\dfrac{1}{2c_2} \end{pmatrix}.$$

where

$$c_1 = \sqrt{g\frac{h_{1,i} + h_{1,i+1}}{2}}, \qquad c_2 = \sqrt{g\frac{h_{2,i} + h_{2,i+1}}{2}}.$$

It should be noted that the finite volume SRNHS method can be interpreted as a predictor-corrector procedure. In the predictor stage, the averaged states $\mathbf{W}_{i+1/2}^n$ are computed whereas, the solution $\mathbf{W}_i^{n+1}$ is updated in the corrector stage.

2.2 Nonlinear filter procedure

Non-physical oscillations are expected to be appeared in the vicinity of the shocks and hydraulic jumps. In the present work, to remove these inevitable oscillations we incorporate a filter proposed in [17] for our composite scheme. The main features of this filter are: (i) identify the nodes where the solution tends to oscillate, (ii) determine whether a particular node is an undershoot or overshoot, the flow variables need to be correspondingly lifted or reduced, (iii) conserve mass by balancing a correction (addition/subtraction) at node with an equal and opposite correction (subtraction/addition) from an adjacent node, and (iv) ensure portability where the formulation is independent of the basic numerical scheme.

For our composite scheme, the nonlinear filter is applied to each physical variable $v \in \{h_1, u_1, h_2, u_2\}$ at each gridpoint in which v_i is a local extrema *i.e.*, $d^+ d^- < 0$, where the differences d^+ and d^- are defined as

$$d^+ = v_{i+1} - v_i, \qquad d^- = v_i - v_{i-1}.$$

Hence, a correction term is added to the variable v_j as follows

$$v_i = v_i + \delta_i \text{sign}(d^+), \qquad \text{if} \quad d^+ d^- < 0,$$

where δ_j is a limiting parameter defined by

$$\delta_i = \min \left(\min \left(|d^+|, |d^-| \right), \frac{1}{2} \max \left(|d^+|, |d^-| \right) \right).$$

In addition, to retain conservation, one of v_{i-1} or v_{i+1} must be corrected in the opposite sense according to

$$v_j = v_j - \delta_i \text{sign}(d^+), \tag{14}$$

with

$$j = \begin{cases} i+1, & \text{if} \quad d^+ > d^-, \\ i-1, & \text{otherwise.} \end{cases}$$

Notice that the correction (14) is applied for both neighboring cells to $[x_{i-1/2}, x_{i+1/2}]$ where the local extrema is located. Here the amount of the correction included is distributed among the left solution v_{i-1} and the right solution v_{i+1} depending on the values of the distances d^- and d^+, respectively. By doing so the conservation property of the scheme is preserved and oscillatory behavior is removed near shock areas. In addition the above filter is the simplest one presented in [17] but can be extended to obtain a TVD-enforcing filter. The TVD filtering procedure adopted for our system of equations cannot be explicitly presented in a pseudo-language algorithm, which corresponds to the implementation of the nonlinear filtering similar to algorithm described below and for brevity in presentation, we refer the reader to [17] where the algorithm was described in details. However, one must be careful when choosing the filter, as it may add numerical dissipation. In fact, too much filtering, may destroy the solution and it often suffices to apply the filter after each full timestep or even after several timesteps, depending on the nature of the problem.

Let $\mathcal{L}_{SRNHS}$ be the time-splitting operator in (9) mapping grid data at time n to the data at time $n+1$, and let $\mathcal{L}_F$ be the selected filter operator. Then, the difference operator S_k defined by doing $k-1$ applications of $\mathcal{L}_{SRNHS}$ followed by one application of $\mathcal{L}_F$ is defined as

$$S_k = \mathcal{L}_F \circ \underbrace{\mathcal{L}_{SRNHS} \circ \mathcal{L}_{SRNHS} \circ \cdots \circ \mathcal{L}_{SRNHS}}_{(k-1) \text{ times}}.$$

Thus, the solution of the two-layer shallow water equations is updated as

$$\mathbf{W}^{n+k} = S_k \, \mathbf{W}^n. \tag{15}$$

The treatment of source terms in the shallow water equations presents a challenge in many numerical methods, compare [7] and further references are therein. In our composite scheme, the approximation of source terms is reconstructed such that the still-water equilibrium (C-property) is satisfied. Note that the system (1) has the steady states at rest [2]

$$u_j = 0, \qquad \partial_x \left(Z + \sum_{k=1}^{j-1} \frac{\rho_k}{\rho_j} h_k + \sum_{k=j}^{2} h_k \right) = 0, \quad j = 1, 2. \tag{16}$$

Hence, a numerical scheme is said to satisfy the C-property for the two-layer model if the conditions

$$u_j = 0, \qquad Z + \sum_{k=1}^{j-1} \frac{\rho_k}{\rho_j} h_k + \sum_{k=j}^{2} h_k = H, \quad j = 1, 2, \tag{17}$$

hold for stationary flows at rest. In (17), H is an arbitrary nonnegative constant. Remark that, if $\rho_1 < \rho_2$, the above condition yields

$$u_1 = u_2 = 0, \quad Z + h_2 = H_2, \quad h_1 = H_1, \tag{18}$$

with H_1 and H_2 are nonnegative constants, whereas if $\rho_1 = \rho_2$, the condition (17) reduces to

$$u_1 = u_2 = 0, \quad Z + h_1 + h_2 = H. \tag{19}$$

Therefore, the treatment of source terms in our composite method is reconstructed such that the condition (19) is preserved at the discretized level. For more details on the discretization of the source terms in the SRNHS solver we refer the reader to [16].

It should also be stressed that according to the study reported in [9], the well-established algebraic balancing technique cannot be extended to the two-layer shallow water model in the presence of interface perturbation due to the effect of an additional term associated with the layer coupling which violates the well-balanced property. In the present study, we also overcome this difficulty by interpreting the the two-layer model (1) as a system of two coupled shallow water problems where the topography in one layer depends on the other layer height (*i.e.* the topography is $Z + h_2$ for the first layer, and $Z + \frac{\rho_1}{\rho_2} h_2$ for the second layer). Note that this is not exactly true as these topographies $Z + h_2$ and $Z + \frac{\rho_1}{\rho_2} h_2$ do depend on time as well. However, this happens to be true when using the considered time-splitting method as demonstrated in the results presented in our study. Hence, the difficulty of nonconservative products disappears apparently and thus, we discretized the topography in each layer independently of the other as follow

$$\frac{(h_1 u_1)^{n+1} - (h_1 u_1)^n}{\Delta t} = -g \frac{(h_{1,i-1}^n + 2h_{1,i}^n + h_{1,i+1}^n)}{8\Delta x} \left[(h_{2,i+1} - h_{2,i-1})^n + (Z_{i+1} - Z_{i-1}) \right],$$

$$\frac{(h_2 u_2)^{n+1} - (h_2 u_2)^n}{\Delta t} = -g \frac{(h_{2,i-1}^n + 2h_{2,i}^n + h_{2,i+1}^n)}{8\Delta x} \left[\frac{\rho_1}{\rho_2} (h_{1,i+1}^n - h_{1,i-1}^n) + (Z_{i+1} - Z_{i-1}) \right].$$

In summary, the implementation of the algorithm for the considered nonlinear filter is carried out in the following steps:

$j = 2$
$newind(v, 2, l, j)$

8

while $j < N$ **do**

    $d_1 = v_j - \max(v_{l-1}, ..., v_{j+1})$

    $d_2 = \min(v_{l-1}, ..., v_{j+1}) - v_j$

    if $(\Delta_+ v_j)(\Delta_- v_l) < 0$ and $(d_1 > 0$ or $d_2 < 0)$ **then**

        if $|\Delta_+ v_j| > |\Delta_- v_l|$ **then**

            $d^+ = |\Delta_+ v_j|$

            $d^- = |\Delta_- v_l|$

            $jcorr = j + 1$

            $lcorr = j + 1$

        else

            $d^+ = |\Delta_- v_j|$

            $d^- = |\Delta_+ v_l|$

            $newind(v, l-1, lcorr, jcorr)$

        end if

        $w_1 = j - l + 1$

        $w_2 = jcorr - lcorr + 1$

        $\delta = \min(\delta_-, w_2 \delta_+/(w_1 + w_2), \max(d_1, d_2))$

        $s = sgn(\Delta_+ v_j)$

        for $i = l \rightarrow j$ **do**

            $v_i = v_i + s\delta$

        end for

        for $i = lcorr \rightarrow jcorr$ **do**

            $v_i = v_i - s\delta w_1/w_2$

        end for

        $newind(v, l-1, p, q)$

    else if $(\Delta_+ v_j)(\Delta_- v_l) < 0$ and $(\Delta_+ v_{l-1})(\Delta_- v_p) < 0$ **then**

        $\delta = \min(|\Delta_- v_p|, |\Delta_+ v_{l-1}|/2, |\Delta_+ v_j|)$

        $s = sgn(\Delta_+ v_j)$

        for $i = p \rightarrow l-1$ **do**

            $v_i = v_i - s\delta$

        end for

        for $i = l \rightarrow j$ **do**

            $v_i = v_i + s\delta$

        end for

    else

        if v_j does not need any correction go to $j + 1$

        $newind(v, j+1, l, j)$

    end if

end while

In the above algorithm the function $newind(u, ind, l, j)$ returns the indices (l, j) such that

$$u_{l-1} \neq u_l = u_{l+1} = \cdots = u_j \neq u_{j+1}.$$

In the sequel, we shall use the terminology SRNHS-F(k) to refer to the proposed composite scheme. Note that for $k = 0$ the SRNHS-F(0) reduces to the conventional $\mathcal{L}_{SRNHS}$ operator.

3   Applications and numerical results

To examine the effectiveness and the performance of our composite scheme we present numerical results for several test examples. We illustrate the results for two-layer shallow water flows

Table 1: Errors for the accuracy test problem using different meshes.

M	L^1-error	rate	L^2-error	rate	$L^\infty-$error	rate
300	$4.6141E$-04	—	$5.8592E$-03	—	$1.7599E$-01	—
600	$1.8703E$-04	1.30	$2.6415E$-03	1.14	$9.2250E$-02	0.93
1200	$8.5993E$-05	1.12	$1.2961E$-03	1.07	$5.5999E$-02	0.72
2400	$3.6363E$-05	1.24	$5.5354E$-04	1.22	$1.9296E$-02	1.53

on both flat and non-flat bottom beds. As with all explicit time stepping methods the theoretical maximum stable time step is specified according to the Courant-Friedrichs-Lewy (CFL) condition

$$\Delta t = Cr \frac{\Delta x}{\max\limits_{k=1,\dots,4} \left(|\lambda_k^n| \right)}. \tag{20}$$

where λ_k^n are the approximated eigenvalues in (11) and Cr is a constant to be chosen less than unity. In all the computations reported herein, the Courant number Cr is set to 0.7 and the time stepsize Δt is adjusted at each step according to the stability condition (20).

For comparison reasons, we also compare the results obtained using our composite SRNHS-F(k) scheme to those obtained using the composite LFAD2 and LWLF4 methods proposed in [13]. Here, LFAD2 stands for the Lax-Friedrichs with the anti-diffusion is applied every second time step whereas, LWLF4 refers to the composite Lax-Wendroff Lax-Friedrichs method with a filtering procedure. This filter in LWLF4 is carried out by replacing every fourth Lax-Wendroff step with a Lax-Friedrichs step. More details on these methods can be found in [13] and will not be repeated here.

3.1 Accuracy test problem

We check the accuracy of the proposed composite method for the canonical shallow water equations proposed in [13] for validating two-layer computations. We solve the equations on a fixed bottom topography defined as

$$Z(x) == \begin{cases} b_c \left(1 - \dfrac{x^2}{a^2} \right), & \text{if } \quad -a \leq x \leq a, \\ 0, & \text{otherwise,} \end{cases}$$

where $b_c = 0.65$, $a = 40$ and $g = 1$ in our simulations. At time $t = 0$, we set $h + Z = 1$, $u = 0.7$ and we present numerical results at time $t = 20$. In Figure 2 we present the obtained results for the water free-surface at $t = 20$ using different meshes for the SRNHS-F(2) scheme. As can be seen from the presented results, the moving shock and the rarefaction wave are well resolved by the SRNHS-F(2) scheme. It is clear that for $M = 300$ and $M = 600$, the numerical diffusion is very pronounced in the numerical solutions. This excessive numerical dissipation has been successfully removed in the water height by increasing the values of M up to 2400 for which the shock and rarefaction are better solved by SRNHS-F(2) scheme. Needless to mention that increasing the number of cells M results in an increase of the computational cost in the SRNHS-F(2) method. For the considered number of control volumes $M = 300$, $M = 600$, $M = 1200$ and $M = 2400$ the required CPU time in the SRNH-F(2) method is 0.469, 1.141, 4.297 and 14.672 seconds, respectively.

10
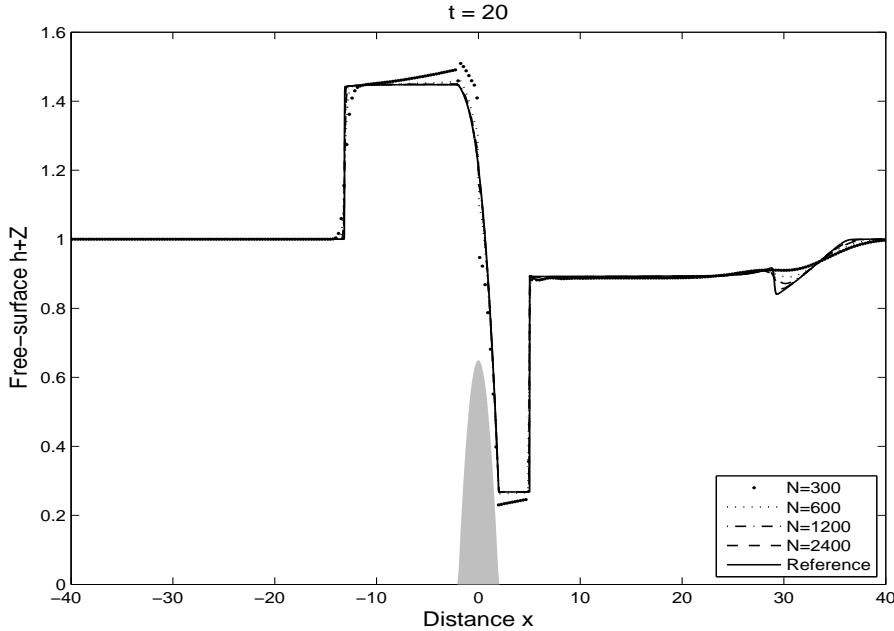
Figure 2: Water free-surface for the accuracy test problem using different meshes.

To quantify the errors in our method a reference solution is computed using LWLF2 on a fine mesh with 4800 control volumes. The obtained results for the L^1-, L^2- and $L^\infty-$error in the water free-surface are listed in Table 1 along with their corresponding convergence rates. It reveals that increasing the number of control volumes in the computational domain results in a decay of all errors. Our composite method SRNHS-F(2) exhibits good convergence behavior for this shallow water problem. As can be seen from the convergence rates presented in Table 1, a first-order accuracy is achieved for this test example in terms of the considered error norms. It is worth to remark that the conclusion from the errors in Table 1 is the fact that although the SRNHS method is second-order accurate the nonlinear filter reduces the convergence rate of the composite scheme to a first-order accuracy.

Next we show the effect of the lost of hyperbolicity on the results computed with our composite SRNHS-F(2) scheme. To this end we consider a test example studied in [2] where we solve the two-layer shallow water on a flat bottom using a density ratio $\dfrac{\rho_1}{\rho_2} = 0.98$ and $g = 9.81$. As initial conditions, we set $u_1(x,0) = 0.6$, $u_2(x,0) = -0.6$,

$$h_2(x,0) = \begin{cases} 0.5 + 0.01\left(1 + \cos(\dfrac{(x-0.5)\pi}{0.1})\right), & \text{if} \quad |x-0.1| < 5, \\ 0.5, & \text{if} \quad |x-0.1| > 5, \end{cases}$$

and $h_1(x,0) + h_2(x,0) = 1$. The computational domain $[0,10]$ is discretized into 1000. The obtained results for the water heights are illustrated in Figure 3 at time $t = 1$. The oscillatory behavior in the results in the central region of the computational domain is to be attributed to the lost of the hyperbolocity in the two-layer shallow water system with the considered density ratio. Indeed, for the considered density ratio, the first-order approximation (5) for the eigenvalues gives complex values and as a consequence, the hyperbolicity of the two-layer system is lost. Although, this example is not physical, the presented results show that the composite method will not break down when it eventually finds complex eigenvalues in other examples.
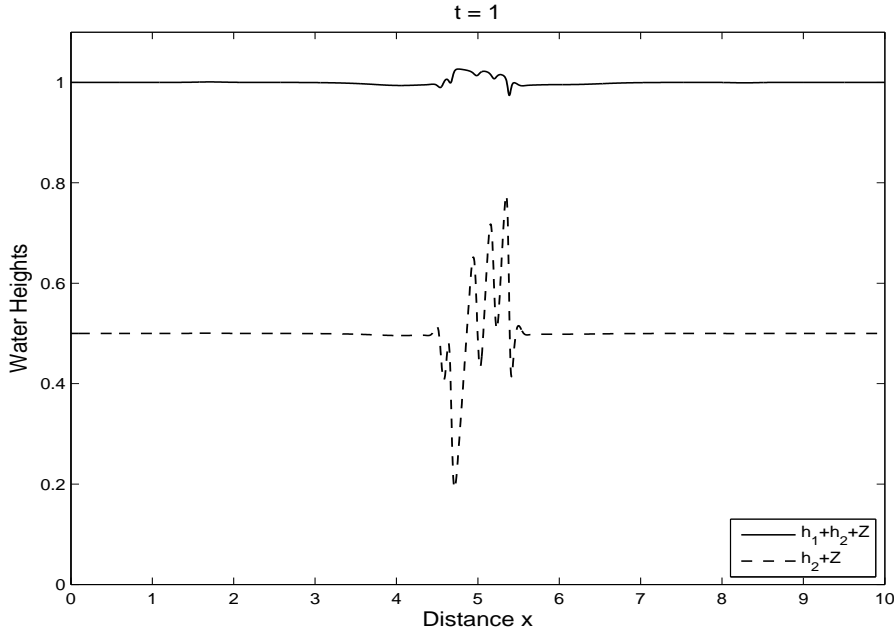
Figure 3: Water heights for the test problem with complex eigenvalues.

3.2 Interface propagation problem

We consider the interface propagation problem studied in [2, 5]. Here we solve the frictionless two-layer shallow water equations (1) in the domain $[0, 10]$ with flat bottom. Initially,

$$(h_1(x,0), h_2(x,0))^T = \begin{cases} (0.2, 1.8)^T, & \text{if} \quad x < 5, \\ (1.8, 0.2)^T, & \text{if} \quad x > 5, \end{cases} \qquad u_1(x,0) = u_2(x,0) = 0.$$

The gravitational constant $g = 9.81$ and the computational domain is discretized into 500 gridpoints. Note that we have imposed initially a jump at the interface, while still having the total water height constant. In Figure 4 we illustrate the water free-surface and the water velocity for $\rho_1/\rho_2 = 0.7$ at time $t = 1$. Figure 5 exhibits the results obtained for $\rho_1/\rho_2 = 0.98$ at $t = 5$. As expected the numerical solution of this problem consists of three constant states connected by two rarefaction waves and two shocks. Observe that increasing the density ratio r from 0.7 to 0.98 results in the elimination of shocks in the water free-surface. As can be seen from the numerical results presented in Figure 4 and Figure 5, the LFAD2 and LWLF4 methods produce diffusive results. For the considered conditions, the proposed composite method is more accurate than the LFAD2 and LWLF4 methods. No oscillations or smearing of shocks have been detected in the computed results. The results depicted in Figure 4 and Figure 5 also show good agreement with those reported in [2, 5]. As can be seen, good behavior is recovered by the composite method for the considered flow conditions in the system (1) without any significant loss of accuracy. The performance of the composite method is very attractive since the computed solutions remain stable and accurate without requiring complicated reconstruction of numerical fluxes.
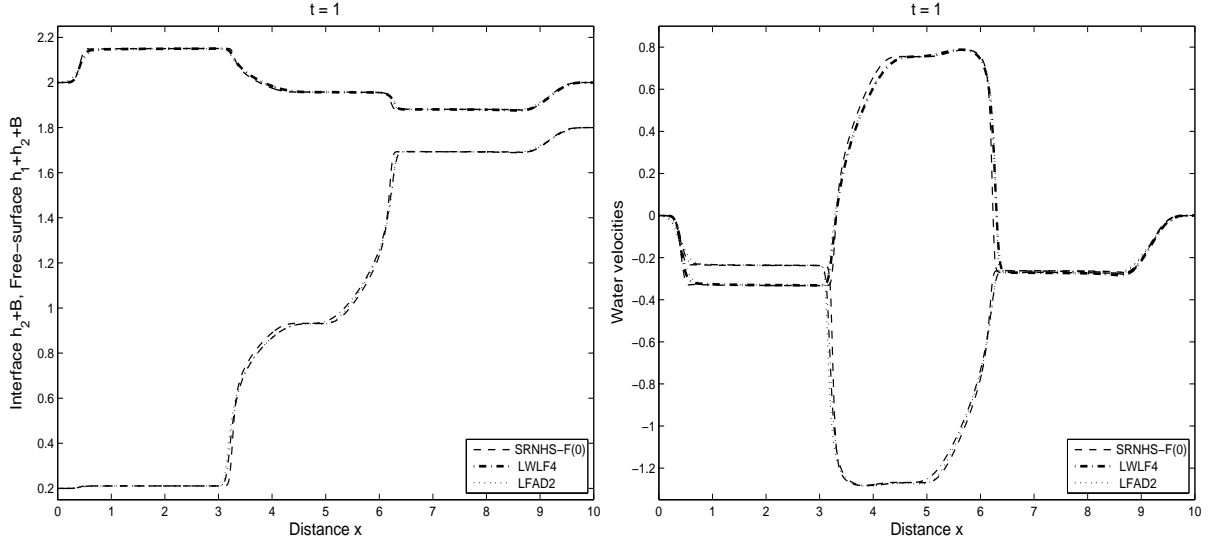
Figure 4: Water free-surface (left) and the water velocity (right) for the interface propagation problem using $\rho_1/\rho_2 = 0.7$ at time $t = 1$.
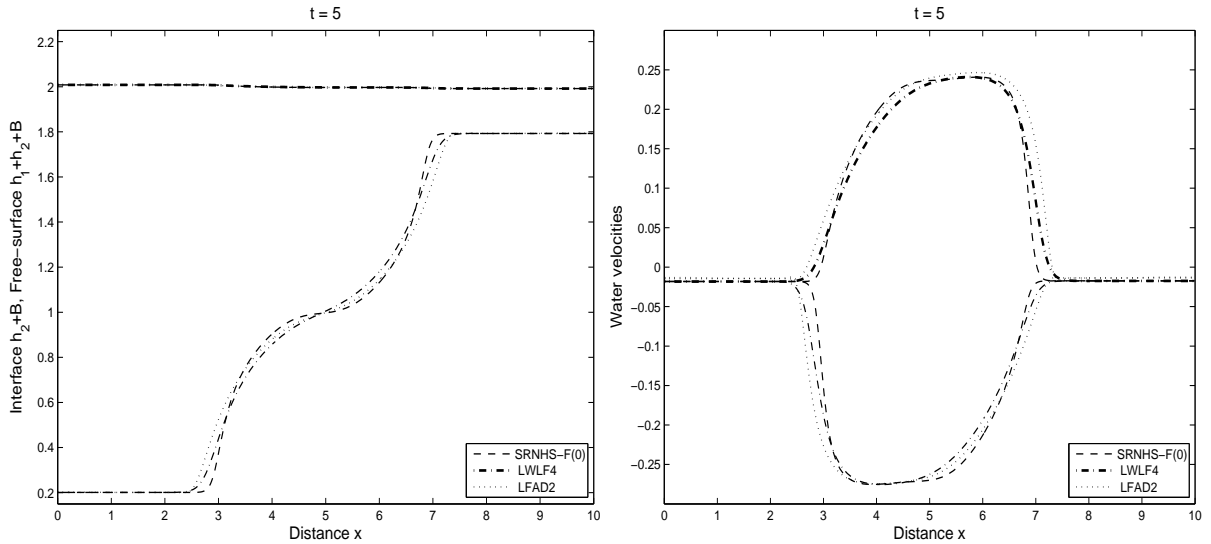
Figure 5: Water free-surface (left) and the water velocity (right) for the interface propagation problem using $\rho_1/\rho_2 = 0.98$ at time $t = 5$.

3.3 Internal dam-break problem

This example solves a problem of internal dam-break modeled by the frictionless two-layer shallow water equations (1) subject to the following initial conditions

$$(h_1(x,0), h_2(x,0))^T = \begin{cases} (0.6, 0.4)^T, & \text{if } x < 5, \\ (0.4, 0.6)^T, & \text{if } x > 5, \end{cases} \qquad u_1(x,0) = u_2(x,0) = 0.$$

The equations are solved in the interval $[0, 10]$ discretized into 1000 gridpoints and the gravitational constant $g = 9.81$. As in the previous test example, we have imposed initially a jump

13

at the interface, while still having the total water height constant. Figure 6 presents the water height and water interface at time $t = 10$ using $\rho_1/\rho_2 = 0.98$. The proposed composite method accurately resolves this internal dam-break problem without exhibiting nonphysical oscillations.
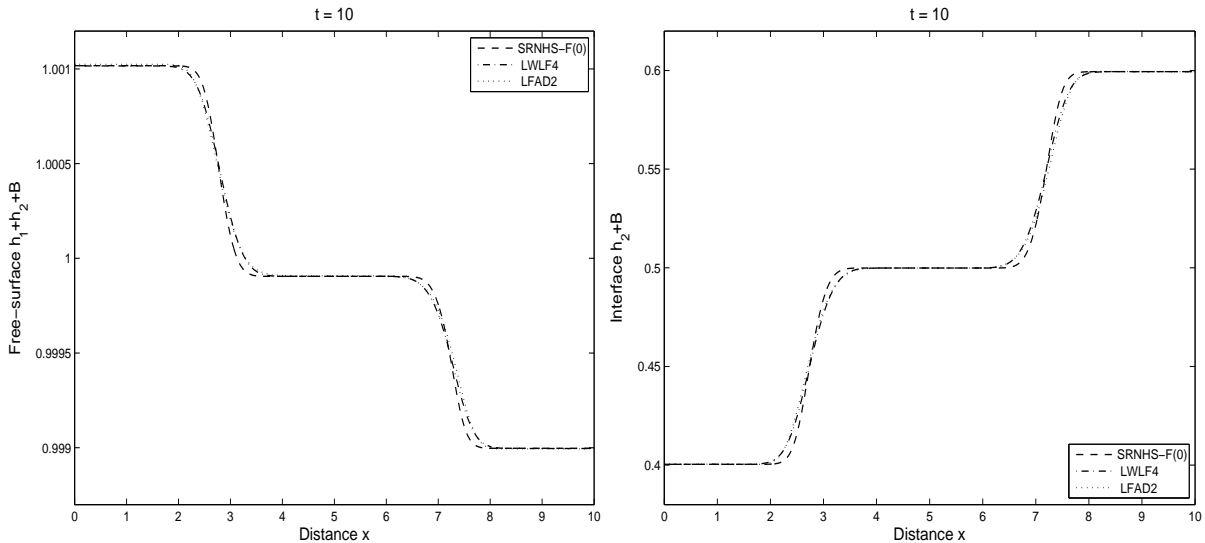
Figure 6: Water free-surface (left) and the water interface (right) for the internal dam-break problem using $\rho_1/\rho_2 = 0.98$ at time $t = 10$.

3.4 Flow over a non-flat bottom

To investigate the ability of our composite method to preserve the correct dynamics solutions, we apply the scheme to a test problem of flow over a non-flat bottom. In this test example the computational domain is $[-20, 20]$ and the bottom topography Z is defined as

$$Z(x) = \begin{cases} b_c \left(1 - \dfrac{x^2}{a^2} \right), & \text{if } -a \leq x \leq a, \\ 0, & \text{otherwise.} \end{cases} \tag{21}$$

The purpose of this test example is to compare the results obtained using the two-layer equations to those obtained using the standard single-layer shallow water equations. Hence, the two-layer shallow water model (1) is solved using the same densities $\rho_1 = \rho_2$ in both layers and initially,

$$h_2(x, 0) = \frac{(1 + b_c)}{2} - Z(x), \qquad h_2(x, 0) = 1, \qquad u_1(x, 0) = u_2(x, 0) = 0.$$

It should be pointed out that if the velocities of both layers remain the same $u_1 = u_2$ then the two-layer shallow water model has to produce the same results as the single-layer shallow water model.

In Figure 7 we show the comparative results for the two-layer and one-layer shallow water models on the computational domain $[-20, 20]$ discretized into 1000 cells using $b_c = 0.2$, $u_0 = 1$ and at times $t = 5$, 10 and 20. Both the two-layer and one-layer models were solved using LWLF4, SRNHS F(2) and LWLF4 methods which give results with negligible difference. All the considered method capture the hydraulic jump in the computed water free-surface without exhibiting non-physical spurious oscillations. The obtained results also show good agreement for the upper water surface obtained by the one-layer and two-layer models.

14
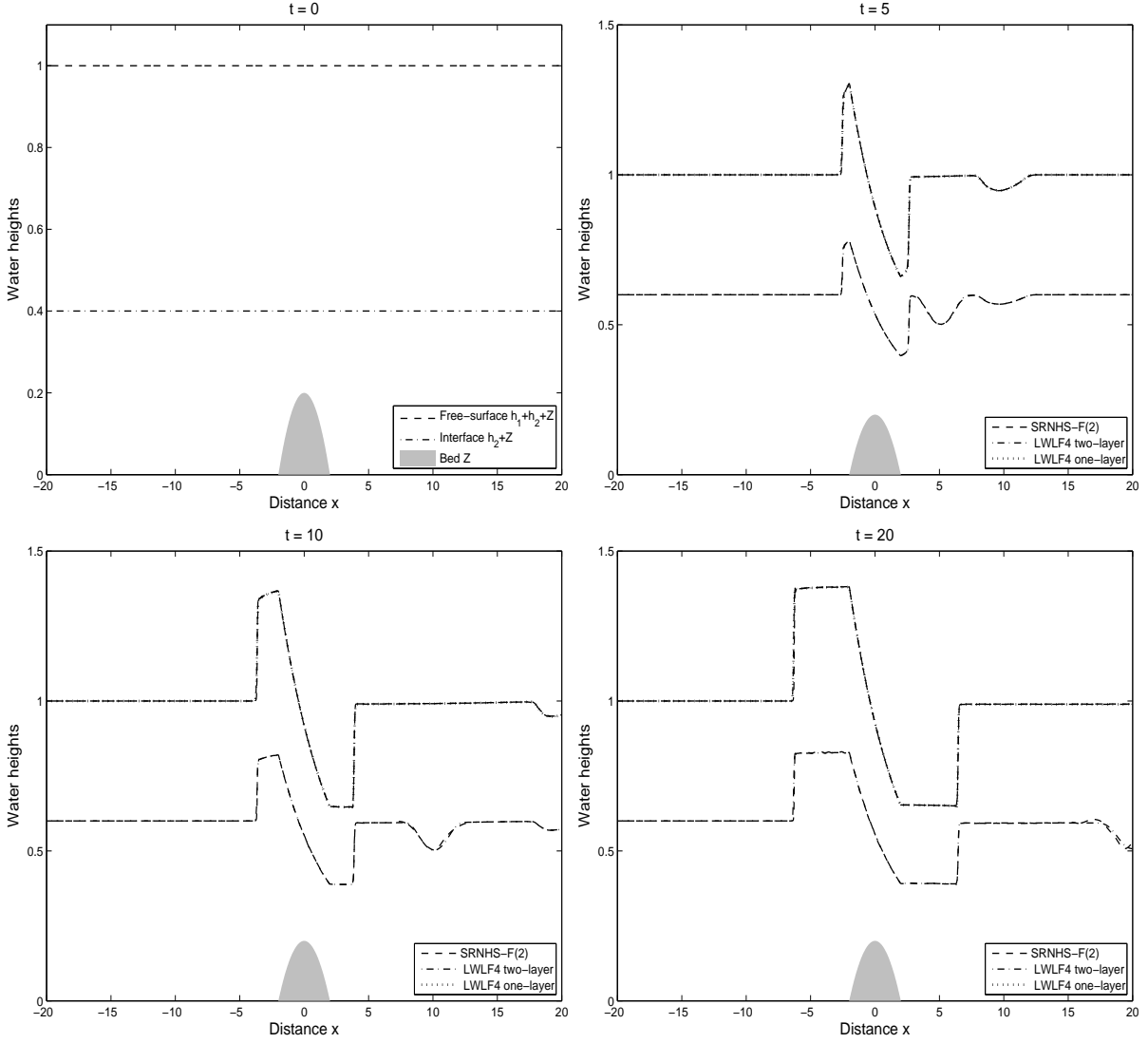
Figure 7: Comparison of water heights for two-layer and single-layer shallow water models in the example of flow over a non-flat bottom at different times.

3.5 Two-layer flow over a hump

We consider an example of two-layer flow over a hump studied in [13, 18]. Here, we solve the frictionless two-layer equations (1) over a hump defined by (21) with $b_c = 0.8$, the gravitational constant $g = 1$, the density ratio is $r = 0.8$, and the initial water heights and velocities

$$h_2(x, 0) = 1 - Z(x), \quad h_1(x, 0) = 1, \quad u_1(x, 0) = u_2(x, 0) = u_0.$$

The equations are solved in the domain $[-20, 20]$ discretized into 1500 cells. In Figure 8 we compare the results obtained using the composite scheme without and with the nonlinear filter. As expected, the nonlinear filter method has been successful in eliminating the nonphysical oscillations near regions of large gradients. It is seen that for the considered flow conditions, the proposed composite scheme accurately resolves the two-layer shallow water flows over non-flat bottom beds. Figure 9 displays the results obtained at time $t = 15$ using the composite scheme and the LFAD2 and LWLF4 methods. Those results obtained at time $t = 60$ are presented in Figure 10. For better sight we also include a zooming over the hump in this figure. It is

15
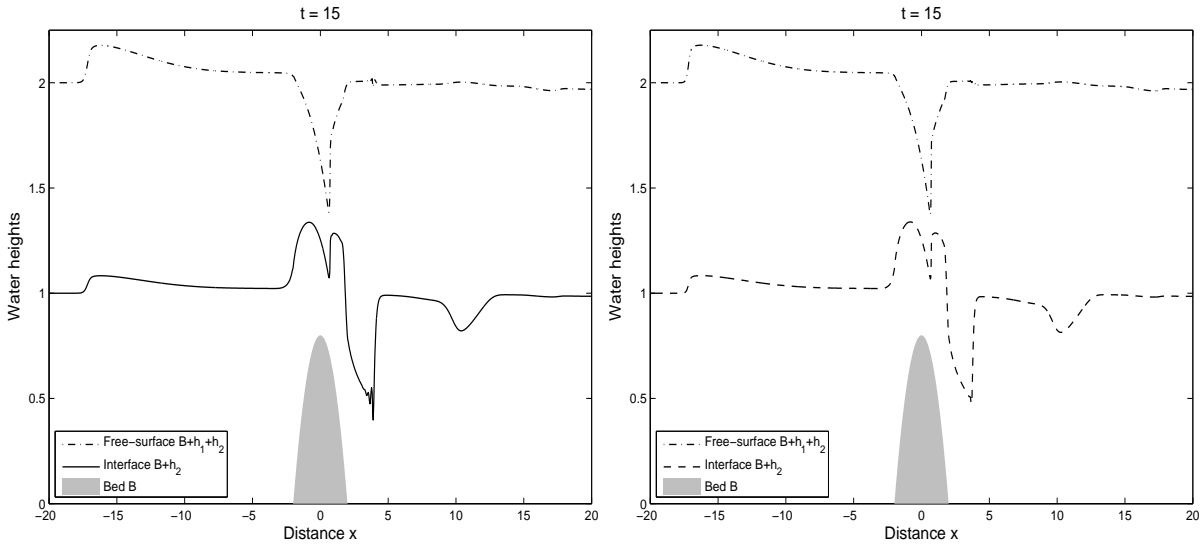
Figure 8: Comparison between results obtained without the filter (left) and with the filter (right) for the two-layer flow over a hump at time $t = 15$.
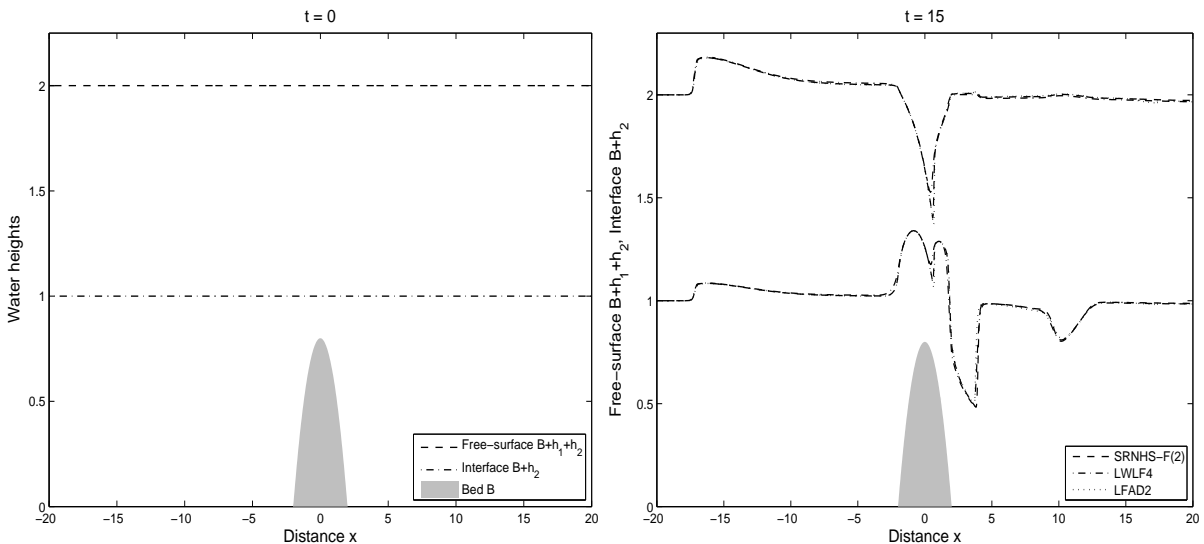
Figure 9: Initial water heights (left) and the computed water heights at time $t = 15$ (right) for the two-layer flow over a hump.

clear from the results presented in this figure that the numerical diffusion is more pronounced in the results obtained using the LFAD2 and LWLF4 methods, compare the hydraulic jumps. Apparently, the overall flow features for this example are preserved with no spurious oscillations appearing in the results obtained using the composite scheme. Obviously, the computed results verify the stability and the shock capturing properties of the proposed nonlinear filter.

3.6 Wind-driven flow problem

To examine the performance of the proposed composite method we consider a test example of two-layer wind-driven flow problem in a lake with non-flat topography studied in [14]. The lake

16
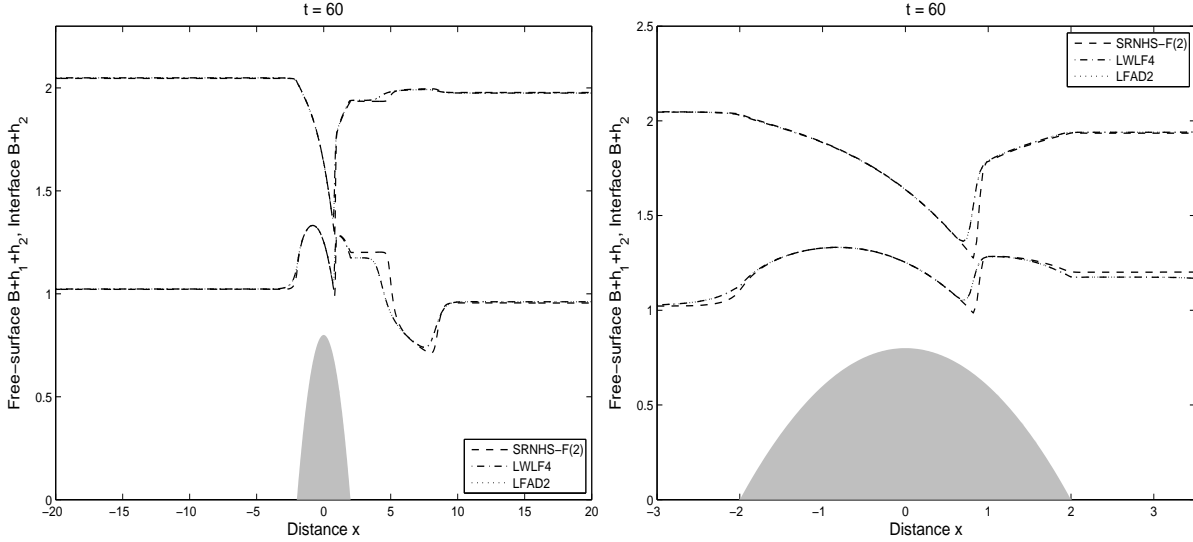
Figure 10: Water heights at time $t = 60$ (left) and a zoom over the hump (right) for the two-layer flow over a hump.

is of length $2000 \ m$ and the bed consists of four bumps defined as

$$Z(x) = \sum_{k=1}^{4} A_k \exp\left(-\left(\frac{x - x_k}{100}\right)^2\right),$$

where $A_1 = A_3 = 0.5$, $A_2 = 1$, $A_4 = 0.25$, $x_1 = 500 \ m$, $x_2 = 800 \ m$, $x_3 = 1100 \ m$ and $x_4 = 1400 \ m$. Initial water level and initial velocity are given as

$$h_2(x, 0) = 4 - Z(x), \qquad h_1(x, 0) = 6.75 - h_2(x, 0) - Z(x),$$

$$u_1(x, 0) = u_2(x, 0) = 0.$$

The selected values for the evaluation of the present method SRNHS-F(0) with $r = 0.8$ are $\rho_a = 1.2 \ kg/m^3$, $g = 9.81 \ m/s^2$ and $nb = 0.035 \ s/m^{1/3}$. Depending on the wind conditions, two situations are simulated namely:

(i) Wind blowing from the east corresponding to $(\omega = -2.1 \ m/s)$.

(ii) Wind blowing from the west corresponding to $(\omega = 2.1 \ m/s)$.

The computational domain is discretized in 500 gridpoints and the computed water free-surface and velocity fields are illustrated at four different instants $t = 250 \ s$, $t = 500 \ s$, $t = 1000 \ s$ and $t = 2000 \ s$. In Figure 11 we present numerical results for the water free-surface and the water velocity obtained using conditions for the wind blowing from the west. Those results obtained for the wind blowing from the east are displayed in Figure 12. In Figure 11 and Figure 12, we also show the topography used in the lake. It is clear that using the considered wind conditions in the two-layer shallow water flow example, the flow exhibits a hydraulic jump with different order of magnitudes near the center of the lake. At the beginning of simulation time, the water flow enters the lake from the eastern boundary and flows towards the eastern exit of the lake. At later time, due to wind effects, the water flow changes the direction pointing towards the eastern coast of the lake. Note that this recirculation features of the water flow can not be captured using the conventional single-layer shallow water equations. A periodic behavior

17
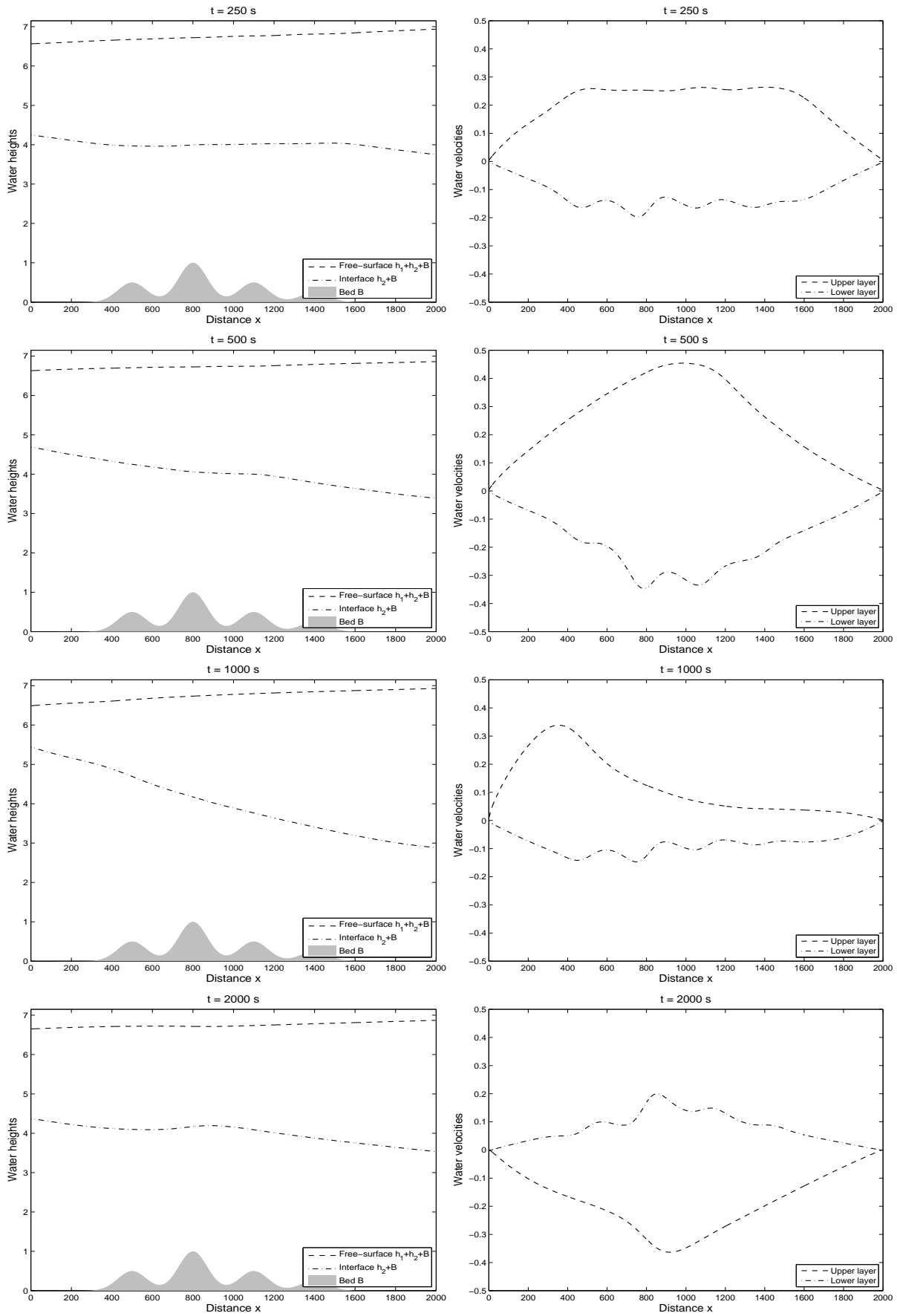
Figure 11: Water free-surface (left column) and water velocity (right column) for blowing wind from the west at four simulation times.
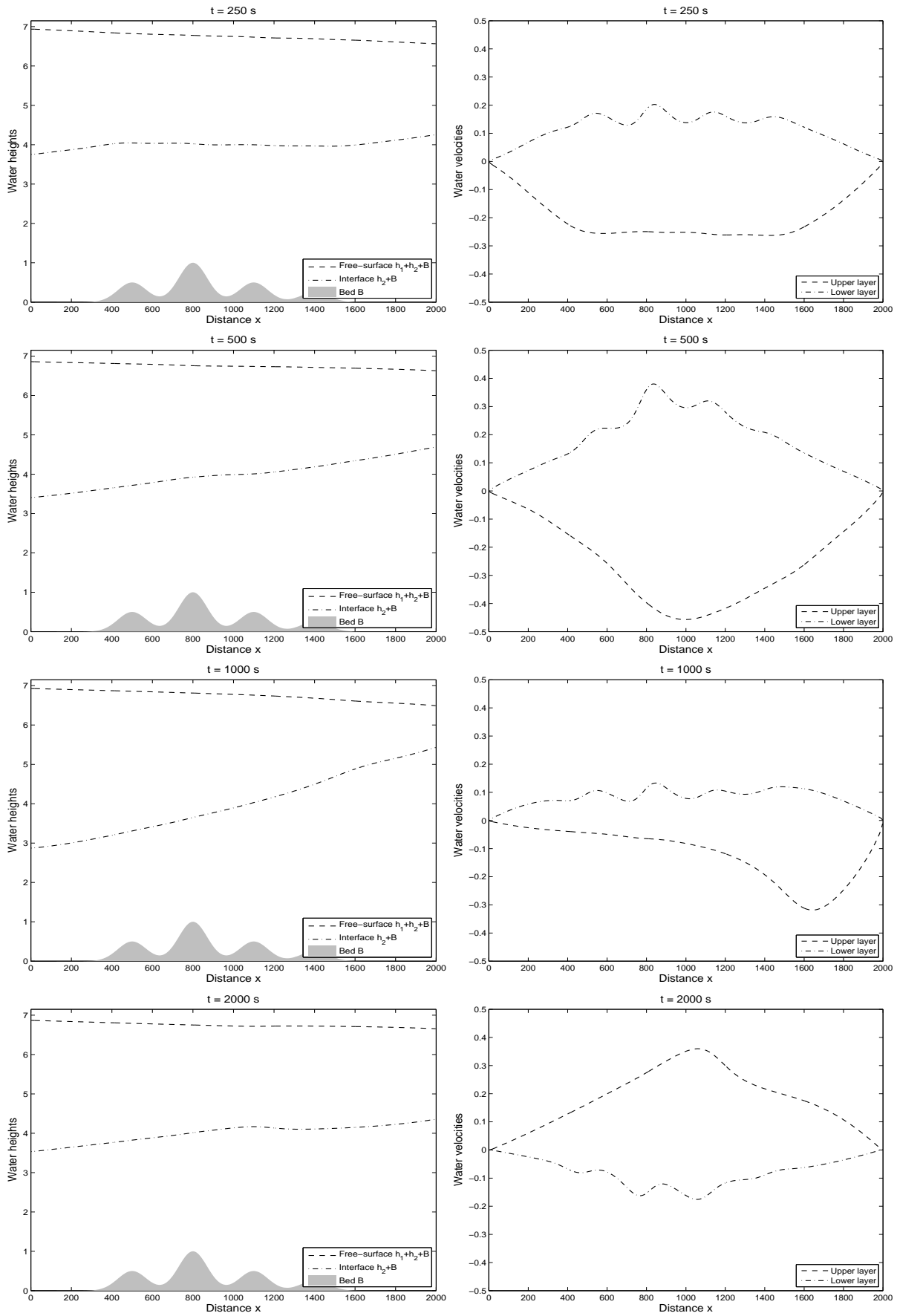
Figure 12: Water free-surface (left column) and water velocity (right column) for blowing wind from the east at four simulation times.

is also detected for the considered two-layer shallow water flow problem subject to the wind blowing from the east and west. These results also show good agreement with those reported in [14]. The proposed composite method performs very satisfactorily for this test problem since it does not diffuse the moving fronts and no spurious oscillations have been detected near steep gradients of the flow field in the computational domain.

4   Conclusions

In this paper we have proposed a new composite scheme for the two-layer shallow water flows with shocks. The proposed finite volume method is a time-splitting procedure and it consists of two stages which can be viewed as a predictor-corrector procedure. In the first stage, the scheme reconstructs the numerical fluxes using the sign matrix of the flux Jacobian in the homogeneous system. In the second stage, the solution is updated using a nonlinear filter in order to obtain a non-oscillatory discretization of the flux gradients and simple treatment of the source terms. Numerical results and applications have been illustrated for several test problems for two-layer shallow water flows on both flat and non-flat bottom beds. The presented results demonstrate the accuracy of the new finite volume method and its capability to simulate water flows in the hydraulic regimes considered. The results make it promising to be applicable also to real situations where, beyond the many sources of complexity, there is a more severe demand for accuracy in predicting the two-layer shallow water flows, which must be performed for long time. Future work will concentrate on developing efficient time integration schemes for the finite volume discretization and extension of this approach to two-layer shallow water flow problems in two space dimensions.

References

[1] J.R. Garratt, Review of drag coefficients over oceans and continents, *Mon. Weather Rev.*, 1977, 105, 915-929.

[2] F. Bouchut and T. Morales, An entropy satisfying scheme for two-layer shallow water equations with uncoupled treatment, *M2AN Math. Model. Numer. Anal.*, 2008, 42, 683-698.

[3] M.J. Castro and T. Chacón and E.D. Nieto and C. Parés, On well-balanced finite volume methods for nonconservative nonhomogeneous hyperbolic systems, *SIAM J. Sci. Comput.*, 2007, 29, 1093-1126.

[4] M.J. Castro and J. Macías and C. Parés, A Q-scheme for a class of systems of coupled conservation laws with source term: Application to a two-layer 1D shallow water system, *M2AN Math. Model. Numer. Anal.*, 2001, 35, 107-127.

[5] M. Dudzinski and M.L. Medvidova, Well-balanced path-consistent finite volume EG schemes for the two-layer shallow water equations, *Computational Science and High Performance Computing.*, 2009, IV, 121-136.

[6] R. Abgrall and S. Karni, Two-layer shallow water systems: a relaxation approach, *SIAM J. Sci. Comput.*, 2009, 31, 1603-1627.

[7] F. Benkhaldoun, I. Elmahi, M. Seaid, A new finite volume method for flux-gradient and source-term balancing in shallow water equations, *Computer Methods in Applied Mechanics and Engineering*, 2010, 199, 49-52.

[8] M.J. Castro, P.G. LeFloch, Muñoz, C. Parés, Why many theories of shock waves are necessary: convergence error in formally path-consistent schemes, *J. Comp. Physics.*, 2008, 227, 8107-8129.

[9] W.K. Lee, A.G.L. Borthwick, P.H. Taylor, On mathematical balancing of a two-layer shallow flow model, in: IAHR Eur. Div. Congress, 1st., IAHR, Edinburgh, 2010.

[10] J. B. Schijf and J. C. Schonfeld. Theoretical considerations on the motion of salt and fresh water. In Proc. of the Minn. Int. Hydraulics Conv., Joint meeting IAHR and Hyd. Div. ASCE., pages 321-333, Sept. 1953.

[11] J. Macías and C. Parés and M.J. Castro, Improvement and generalization of a finite element shallow water solver to multi-layer systems, *Int. J. Numer. Methods Fluids.*, 1999, 31, 1037-1059.

[12] M.J. Castro and J. Macías and C. Parés and J.A. Garciá-Rodríguez and E. Vázquez-Cendoón, A two-layer finite volume model for flows through channels with irregular geometry: computation of maximal exchange solutions. Application to the Strait of Gibraltar, *Commun. Nonlinear Sci. Numer. Simul.*, 2004, 9, 241-249.

[13] R. Liska, B. Wendroff, Analysis and Computation with Stratified Fluid Models, *J. Comp. Physics.*, 1997, 137, 212-244.

[14] E. Audusse and F. Benkhaldoun and J. Sainte-Marie and M. Seaid, Multilayer Saint-Venant equations over movable beds, *Discrete and Continuous Dynamical Systems - Series B.*, 2011, 15, 917-934.

[15] D. Ambrosi, Approximation of shallow water equations by Riemann solvers, *Inter. Journ. for Numerical Methods in Fluids*, 1995, 20, 157-168.

[16] S. Sahmim and F. Benkhaldoun and F. Alcrudo, A Sign Matrix Based Scheme for Quasi-Hyperbolic Non-Homogeneous PDEs with an Analysis of the Convergence Stagnation Problem, *J. Comput. Physics*, 2007, 226, 1753-1783.

[17] B. Engquist and P. Ltstedt and B. Sjgreen, Nonlinear filters for efficient shock computation, *Math.Comp.*, 1989, 186, 509-537.

[18] B. Spinewine and V. Guinot and S. Soares Frazão and Y. Zech, Solution properties and approximate Riemann solvers for two-layer shallow water flow models, *Math.Comp.*, 1989, 186, 509-537.